Summary of the First High-Altitude, Supersonic Flight Dynamics Test for the Low-Density Supersonic Decelerator Project

Ian G. Clark* Mark Adler † and Rob Manning ‡

Jet Propulsion Laboratory, California Institute of Technology, Pasadena, California, 91109

NASA's Low-Density Supersonic Decelerator Project is developing and testing the next generation of supersonic aerodynamic decelerators for planetary entry. A key element of that development is the testing of full-scale articles in conditions relevant to their intended use, primarily the tenuous Mars atmosphere. To achieve this testing, the LDSD project developed a test architecture similar to that used by the Viking Project in the early 1970's for the qualification of their supersonic parachute. A large, helium filled scientific balloon is used to hoist a 4.7 m blunt body test vehicle to an altitude of approximately 32 kilometers. The test vehicle is released from the balloon, spun up for gyroscopic stability, and accelerated to over four times the speed of sound and an altitude of 50 kilometers using a large solid rocket motor. Once at those conditions, the vehicle is despun and the test period begins.

The first flight of this architecture occurred on June 28th of 2014. Though primarily a shake out flight of the new test system, the flight was also able to achieve an early test of two of the LDSD technologies, a large 6 m diameter Supersonic Inflatable Aerodynamic Decelerator (SIAD) and a large, 30.5 m nominal diameter supersonic parachute. This paper summarizes this first flight.

I. Introduction

In 1976 the twin Viking spacecraft became the first spacecraft to successfully land on the surface of Mars. The technology set utilized by Viking, namely a rigid blunt body aeroshell, a supersonic parachute, and a propulsion based terminal descent system, is largely the same one used in the subsequent four decades of Mars spacecraft. Although numerous improvements have been made in the area of hypersonic guidance and terminal descent systems, the supersonic parachute used by Viking is still used consistently. With the successful landing of the Mars Science Laboratory Curiosity rover, it is likely that the landed mass and altitude capabilities of the Viking heritage supersonic decelerator is saturated. Future missions seeking to land greater mass or access higher altitudes will require new supersonic decelerators.

In 2012 NASA initiated the Low-Density Supersonic Decelerator (LDSD) project to develop a new generation of supersonic aerodynamic decelerators. As part of the LDSD project, several new ground-based test architectures were developed for performing structural testing of the decelerators. However, to fully evaluate deployment, inflation, and supersonic and subsonic aerodynamic behaviors, a full-scale flight test was required at conditions relevant to how the technologies would be utilized at Mars. This test series, referred to as the Supersonic Flight Dynamics Test (SFDT), utilizes a test architecture similar to the Viking Balloon Launched Decelerator Test (BLDT) series of 1972.[1] This architecture is outlined in Figure 1.

For a nominal mission, a large helium balloon is used to hoist a 4.7 m diameter blunt body test vehicle to an altitude of over 36 km. The test vehicle is released from the balloon, spun-up for stability, and a Star-48 solid rocket motor ignited. The motor accelerates the test vehicle to approximately Mach 4 and an altitude of 50 km. Upon burn-out, the vehicle is despun and the primary test phase begins. Shortly thereafter, the

*LDSD Principal Investigator, AIAA Member
†LDSD Project Manager, AIAA Associate Fellow
‡LDSD Chief Engineer, AIAA Member

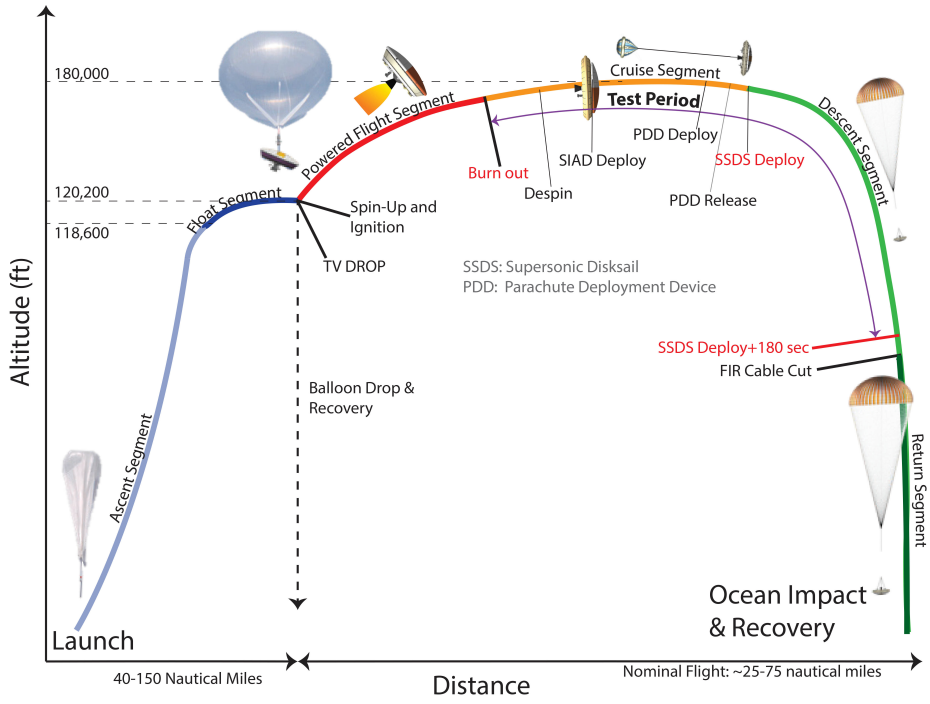

Figure 1. Overview of the LDSD Supersonic Flight Dynamics Test architecture

first of the technologies, a Supersonic Inflatable Aerodynamic Decelerator (SIAD) is deployed. Later in the flight, the Parachute Deployment Device (PDD) is mortar fired, inflated, and subsequently used as a pilot device to extract and deploy a large supersonic parachute from the test vehicle. The parachute decelerates the vehicle to subsonic conditions and the vehicle descends to the ocean for recovery.

The first of these tests, SFDT-1, was conducted on June 28th of 2014 with a balloon launch from the Pacific Missile Range Facility on Kauai, Hawaii. This paper provides a summary of the results of the first test, including balloon launch and float, flight and performance of the SFDT-1 test vehicle, and performance of the technologies tested. This paper focuses on giving a summary of the results from that test. A number of prior or recent papers are available that provide greater details on specific test architecture components or technology results. For example, specifics on the design of the test vehicle and technologies are available in References 2, 3, 4, and 5.

A. Test Objectives

The first SFDT flight was intended as a shakeout flight of the test architecture in preparation for follow-on tests that are specifically for testing the LDSD technologies. A set of minimum success criteria were established as part of this shakeout.

1. Launch with a Star-48 on a balloon from PMRF to float altitude.
2. Conduct a powered flight, demonstrating the ability to target test Mach and dynamic pressure requirements.
3. Collect real-time telemetry from the test vehicle sufficient to assess the powered flight objective and to demonstrate the operation of all RF links.
4. Recover the balloon envelope from the ocean for disposal.

The minimum success criteria were established so as to not require flight of the LDSD decelerators for the first SFDT flight. However, the technologies were available for testing and incorporated onto the test vehicle to attempt an early test of the technologies. Thus, in addition to the minimum success criteria, a secondary set of goals related to the technologies were established.

- Deploy and collect data on the operation and dynamics of the SIAD-R.
- Deploy and collect data on the operation and dynamics of the SSDS parachute.
- Fly the camera mast assembly and other SIAD and SSDS sensors.
- Recover the test vehicle and/or flight image recorder from the ocean.

II. Technology Overview

The Low-Density Supersonic Decelerator (LDSD) Project is developing three new aerodynamic decelerators that are targeted for use in future Mars missions. Two of these devices are supersonic inflatable aerodynamic decelerators (SIADs) and the third is a new supersonic parachute, a supersonic Disksail (SSDS). Each of the two SIADs is named for the class of mission for which it is envisioned to be used for, either robotic class missions (SIAD-R) or exploration class missions (SIAD-E). As a combined SIAD/parachute system, these technologies will allow for increases in landed mass, landed altitude, and landed accuracy beyond what is presently possible with the heritage set of decelerator technologies.

A SIAD is a class of aerodynamic decelerator that is intended to alter the aerodynamic characteristics of an entry vehicle, typically by augmenting drag or lift and/or improving the stability of the entry vehicle. Since they are inflated structures, SIADs provide benefits in mass and packaging and allow for increases in the aerodynamic surfaces of an entry vehicle beyond those provided by a rigid aeroshell constrained to fit within a launch vehicle fairing. As a supersonic decelerator, they are deployed well after the peak heating and deceleration phase but at Mach numbers above those for which parachutes can be used. In that manner, they provide a bridge from hypersonic entry to a Mach and dynamic pressure regime in which a parachute may be used.

A. SIAD-R

The robotic class SIAD consists of an inflated torus with a total diameter of 6 m. The design of SIAD-R is intended to provide an inflated structure that can be pressurized sufficiently to exhibit little or no change in shape when operating in a supersonic flowfield. This feature greatly simplifies the qualification and testing that would be necessary prior to incorporation on a flight mission. For example, since SIAD-R behaves as a rigid structure, aerodynamic characterization can still be performed used traditional techniques that assume rigidity like CFD, subscale wind tunnel testing, and ballistic range testing.

Though primarily an inflated torus, the SIAD-R design has a number of features, shown in Figure 2, designed to improve performance and rigidity. The burble fence on the periphery of the SIAD provides a location of uniform flow separation that improves the stability of the vehicle, particularly at lower supersonic and transonic conditions. The primary torus also contains a series of internal cords that provide additional preload and stiffness in the structure and help resist axial deflection and rotation of the torus under large aerodynamic loads.

The SIAD is constructed primarily from 400-denier Kevlar-29 as the woven broadcloth material with a coating of Silicone RTV. The structure is fabricated using 27 gores sewn together to approximate a circular cross section. Inflation of SIAD-R is achieved using an on-board inflation system of 18 gas generators spaced. The gas generators are fired in two separate groups, an initial lower pressure firing and a subsequent high pressure firing. The low pressure firing uses 9 gas generators consisting of canisters of Nitrogen pressurized to approximately 6 kPa (0.87 psi), while the high pressure firing uses actual combustion products. The gas generators are installed in pairs, with a low and high pressure paired in 40° intervals around the vehicle.

To achieve its rigidity, the SIAD is pressurized to a peak inflation pressure of approximately 31 kPa (4.5 psi). The relatively small size of the SIAD also allows for a rapid inflation of less than one second, thereby minimizing disturbances on the entry vehicle.

B. Supersonic Disksail Parachute

The parachute tested on SFDT-1 is a 96 gore, 30.5 m D_0 Supersonic Disksail (SSDS), shown in Figure 3. The Disksail parachute merges design elements of both a Ringsail parachute and a Disk-Gap-Band (DGB) parachute. The design began with a 22 panel, 96-gore design for a 33.5 m D_0 Ringsail parachute tested as part of the 2005 Subsonic Parachute Technology Task (SPTT).[6,7] The smaller Disksail design reduces the

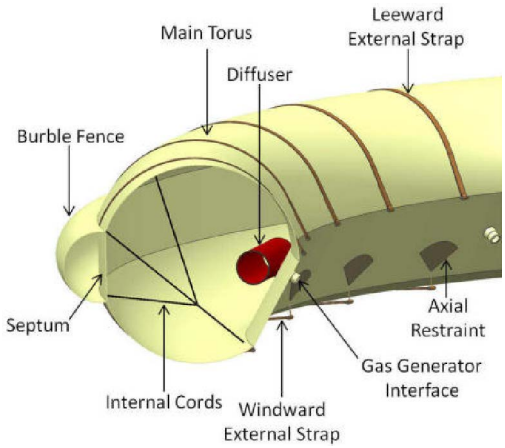

Figure 2. Design features of the robotic class SIAD flown on SFDT-1.

base number of panels to 20 and subsequently replaces the upper 9 panels of the crown with a flat circular disk. The remaining 11 panels constitute sails of increasing fullness, with panels 10-12 having 6% fullness and panels 13-19 having 12% fullness. Panel 20 contains zero fullness, as per typical Ringsail design. Two gaps are present, one large gap at the edge of the disk and another shorter gap between the 15th and 16th panels. The parachute has an as designed geometric porosity of 13.69%, though the as-built geometric porosity of the canopy tested was estimated as 13.06%.

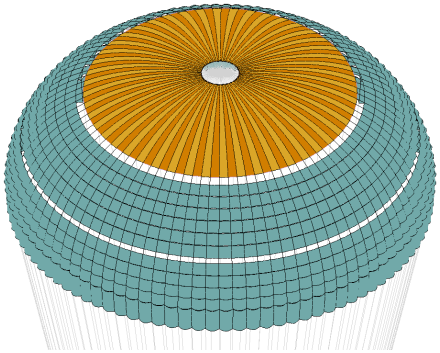

Figure 3. Supersonic Disksail parachute flown on SFDT-1.

Construction of the parachute utilizes Kevlar for the radial and circumferential skeleton. The circumferentials are made from 550 lbf strength, 0.5 in wide Kevlar tape, at the trailing edge of each of the sails. The leading edge of the disk portion of the canopy includes an 800 lbf, 0.5 in wide Kevlar Tape. The radial tapes and skirt band were constructed from 2500 lbf, 1 in wide Kevlar tape. The 96 suspension lines and 48 vent lines were each 2100 lbf Technora cord. The vent band was a 6000 lbf Nylon webbing.

Sail panels of the parachute are made from 1.2 oz/yd^2 PIA-C-44378 Type I (aka F-111) ripstop Nylop with a minimum specified strength of 45 lbf/in. The disk is constructed predominantly of PIA-C-44378 with the exception of a region near the vent constructed from 1.9 oz/yd^2 Diamond Weave ripstop Nylon, which has a minimum specified strength of 80 lbf/in in the warp direction and 85 lbf/in in the fill direction. Low or zero-permeability materials were intentionally selected for parachute construction. The nominal permeability of PIA-C-44378 is 0 - 5 cfm while the Diamond Weave permeability is 20 - 50 cfm. Because of this, the total porosity, including the effects of material permeability, of the Disksail should be very close to the geometric porosity.

The parachute was packed in a two stage deployment bag, with the canopy and approximately 8 m of suspension lines packed into an inner bag and the remainder of the suspension lines packed into an outer bag. The achieved density of the pack was calculated as 552.6 kg/m^3 (34.5 lbm/ft^3). After deployment, the inner bag remained attached to the parachute vent lines while the outer bag remained with the ballute.

C. Parachute Deployment Device

Although not [illegible] was not one of the primary technologies being tested by LDSD, deployment of the SSDS required development of a trailing ballute Parachute Deployment Device (PDD), shown in Figure 4 below. The ballute served as a supersonic pilot device to extract the parachute off of the back of the test vehicle. The basic design was [illegible] 4.4 m diameter, trailing isotensoid of a design similar to prior ballutes tested by NASA (e.g. References 8 and 9).

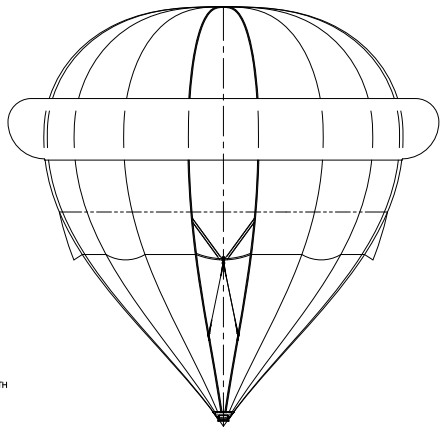

Figure 4. Ballute Parachute Deployment Device used on SFDT-1.

The geometry of the ballute included a 10% burble fence such that the core diameter of the isotensoid was 4.0 m. The inclusion of the burble fence increased the total diameter to 4.4 m. The burble fence is a feature historically common to ballutes that provides a clean separation point and improves stability of the device.

The ballute was designed such that primary inflation is achieved through the use of ram-air inlets. However, an inflation aid device was also incorporated into the ballute design to reduce the risk of failed inflation, such as that observed on a prior NASA test of a 5.49 m diameter ballute (Reference 8). The inflation aid consisted of a water/methanol mixture and was sized to provide at least half of the expected inflation pressure, depending on the conditions of deployment. The ballute was built with 16 ram-air inlets, one on each of two different designs. Every other gore of the ballute had an inlet that stood approximately 1 [illegible] the surface of the ballute while the remaining half of the inlets were flush-mounted (e.g. 0% fullness) with the curvature of the ballute. If the ballute was not fully pressurized, the flush-mounted inlets would serve to provide additional inlet area to facilitate inflation. Tethers attached to the leading edge of the each of the raised inlets were used to ensure that the inlets would not fold back.

The ballute broadcloth was a plain 60 x 60 weave, 200 denier Kevlar 29 cloth with a thin coating of clear KS-1100T Silicone. The uncoated areal density of the broadcloth was measured as 3.14 oz/yd^2 and the coated areal density was 4.17 oz/yd^2. Meridian tapes of 625 lbf Kevlar were used as reinforcement. A trailing distance of 42 m from the maximum diameter of the deployed SIAD-R to the nose of the ballute was achieved using a combination of 5.5 m long triple bridle legs and a roughly 36.5 m long riser. The riser was a 12,500 lbf Kevlar web (PIA-87130 Type VI, Class 11, 1 in. wide) and the triple bridle legs were two legs of 7000 lbf Kevlar webbing (PIA-87130 Type VI Class 9a, 1 in. wide) and a leg of 12,500 lb Kevlar webbing. Attached to the stronger of the three bridle legs was a lazy leg connected to the parachute pack. When the ballute triple bridle is cut, the lazy leg extracts the parachute pack from the back of the vehicle.

The ballute and inflation aid were packed into a single deployment bag with an estimated packing density of 661.6 kg/m^3 (41.3 lbm/ft^3).

III. Instrumentation

The SFDT-1 Test Vehicle (TV) was equipped with scientific instrumentation to observe the trajectory, aerodynamics, and performance of both the test vehicle and test articles. Although there was additional instrumentation associated with vehicle diagnostics, it is not discussed herein. Tabular descriptions of the

metric and imagery instrumentation accuracy and specifications are shown in Tables 1 and 2.

Table 1. Metric Instrumentation Accuracy

Device	Sample Rate	Location
GLN-MAC IMU	400 Hz	
Javad G2T GPS	10 Hz	
SIAD Surface Thermocouples	50 Hz	Gores 2, 11, 20 †‡
SIAD Internal Gas Thermocouples	50 Hz	Gores 2, 11, 20 †
SIAD Internal Pressure Transducers	1 kHz	Gores 2, 11, 20 †
SIAD Leeward Load Cells	1 kHz	Gores 2, 11, 20 †
PDD Load Cells	1 kHz	PDD Bridle Legs
SSDS Load Cells	1 kHz	SSDS Bridle Legs

† See Figure 6 for the SIAD gore labels
‡ See Figure 7 for the surface SIAD thermocouple configuration

Table 2. Imagery Instrumentation Accuracy

Camera	FPS	Location	Accuracy	FOV
SSDS high-speed	135 fps	Camera mast, aft-pointed	2.27 cm/px @ 70m	38x38 deg
SSDS high-resolution	16 fps	Camera mast, aft-pointed	1.18 cm/px @ 70m	48x37 deg
Panoramic Camera	135 fps	Camera mast, parabolic mirror	N/A	N/A
Internal SIAD	44 fps	Gore 18 †	N/A	21x16 deg
Situational Video 1	30 fps	Top deck, centerline-pointed	N/A	69.5x118.2 deg
Situational Video 2	30 fps	Camera mast, +X pointed	N/A	69.5x118.2 deg
Situational Video 3	30 fps	Camera mast, -X pointed	N/A	69.5x118.2 deg
Situational Video 4	30 fps	Camera mast, aft-pointed	N/A	69.5x118.2 deg

† See Figure 6 for the SIAD gore labels

A. Inertial Measurement Unit

The SFDT-1 Test Vehicle (TV) flew one inertial measurement unit, a Gimbaled LN-200 with Miniature Airborne Computer (GLN-MAC).

The GLN-MAC has a single gimbal that is approximately aligned with the roll axis of the TV. This allows the internal LN-200 to stay primarily inertially fixed during the powered phase of the flight, while the vehicle rotates around it at approximately 300 degrees per second. The GLN-MAC provides the following data at 400 Hz that is used directly in trajectory and aerodynamic reconstruction: rotational delta-thetas from the gyroscopes about the LN-200 X, Y, and Z instrument axes, translational delta-velocities from the accelerometers in the LN-200 X, Y, and Z instrument axes, and the gimbal position about the GLN-MAC X platform axis.

B. GPS Unit

The SFDT-1 TV flew one GPS unit, a Javad G2T, with two diametrically-opposed antennas, mounted on the shoulder of the vehicle. In pre-flight simulations, it was found that the GPS had to perform better than 30 meters and 9 meters/second, for position and velocity, respectively, to meet trajectory reconstruction requirements. It was predicted that the GPS would lose satellite lock during the powered spin phase of the flight, where the vehicle was expected to spin at approximately 300 deg/s. During the spin phase, the GPS unit did lose lock, but regained it within 4 seconds of spinning down. The GPS unit also performed much better than the required position and velocity uncertainty.

Figure 5. GLN-MAC Inertial Measurement Unit

C. SIAD Instrumentation

1. SIAD Surface Thermocouples

The 21 surface thermocouples were grouped in sets of 7 thermocouples, located at three circumferential locations on the SIAD, at gores 2, 11, and 20. See Figure 6 for the gore configuration and numbering scheme. At each gore, the thermocouples were installed in a consistent configuration, as shown in Figure 7.

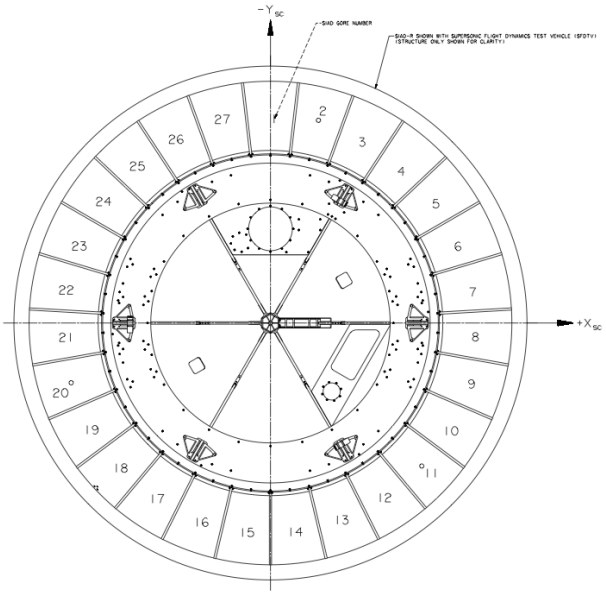

Figure 6. SIAD gore configuration

SIAD Internal Gas Thermocouples The 3 internal gas thermocouples were located at the same gores as the surface thermocouples, gores 2, 11, and 20, as shown in Figure 6. Due to construction of the SIAD and thermocouple mounting, these may not be reading the true gas temperature, and may have sensing some surface conductive heating.

SIAD Internal Pressure Transducers The 3 internal pressure transducers were located at the same gores as the thermocouples, gores 2, 11, and 20.

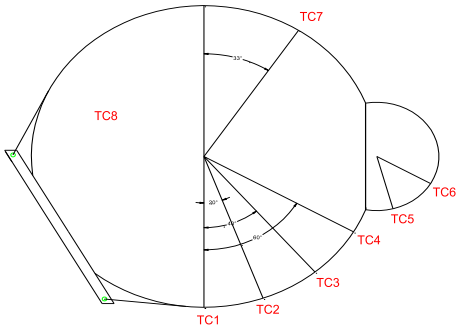

Figure 7. SIAD thermocouples in the same configuration at each gore

Internal SIAD Camera The internal camera was installed at gore 18 that recorded the position of 4 LEDs. This provided both axial translation and rotational deflection of the SIAD during the science phase of the mission. The internal camera recorded at 44 frames per second.

High-speed Panoramic Camera The panoramic camera, which was mounted on the aft-end of the camera mast, was pointed directly aft, into a JPL-built parabolic mirror. This mirror allowed for nearly 360-degree view of the SIAD and TV top deck, with the exception of the mirror support structure and the STAR-48, which occluded the view.

2. Parachute Instrumentation

PDD Load Cells The 3 triple-bridle PDD load cells were located in line with the three triple bridles, near the triple-bridle and top deck interface. Each load cell had a range of 1kN to 4kN, at a frequency of 1 kHz, and an accuracy of 600 N.

SSDS Load Cells The 3 triple-bridle SSDS load cells were located in line with the three triple bridles, near the triple-bridle and top deck interface. Each load cell had a range of 5kN to 267kN, at a frequency of 1 kHz, and an accuracy of 5 kN.

High-resolution and high-speed uplook cameras The high-resolution and high-speed camera system specifications and performance can be found in Table 2. These two cameras were co-boresighted, offset from the TV longitudinal axis by 9 degrees.

3. Range Instrumentation

The test vehicle included a C-band radar beacon with two, diametrically-opposed antennas on the shoulder of the vehicle. The radar beacon allowed for accurate ground tracking of the vehicle during the entirety of the flight, including the expected GPS dropout.

The two radars that were used to track the test vehicle were the ROSA and the DR-COSIP. Table 3 shows their respective accuracies.

Table 3. Range Radar Uncertainties

Uncertainty Source	ROSA	DR-COSIP
Range	2.74 m	4.572 m
Azimuth	0.006 degrees	0.01 degrees
Elevation	0.006 degrees	0.01 degrees

IV. Mission Operations

A. Launch

SFDT1 was conducted out of the US Navy's Pacific Missile Range Facility on the West end of Kauai in the Hawaiian islands, referred to here as the range. The range provides controlled sea and air space to the West of Kauai, as well as communication and tracking assets and vehicle integration facilities. The range has excellent weather conditions near the surface for the launch of large scientific balloons, as well as generally prevailing winds that take the balloon to the West in June and July, away from populated areas.

The trajectory of the balloon phase is determined by the balloon ascent rate as a function of time and the wind direction and speed as a function of altitude. The predicted trajectory must be shown to sufficiently avoid populated areas on and around the islands so that a possible balloon failure at any time during the ascent will not pose a safety hazard. In addition, the predicted balloon trajectory must permit enough time at float altitude and a set of selectable powered-flight azimuths so that the powered flight will be contained within the range boundaries for the test. These safety and operational boundaries are shown in Figure 8, where the balloon ascent must be contained in the yellow boundary.

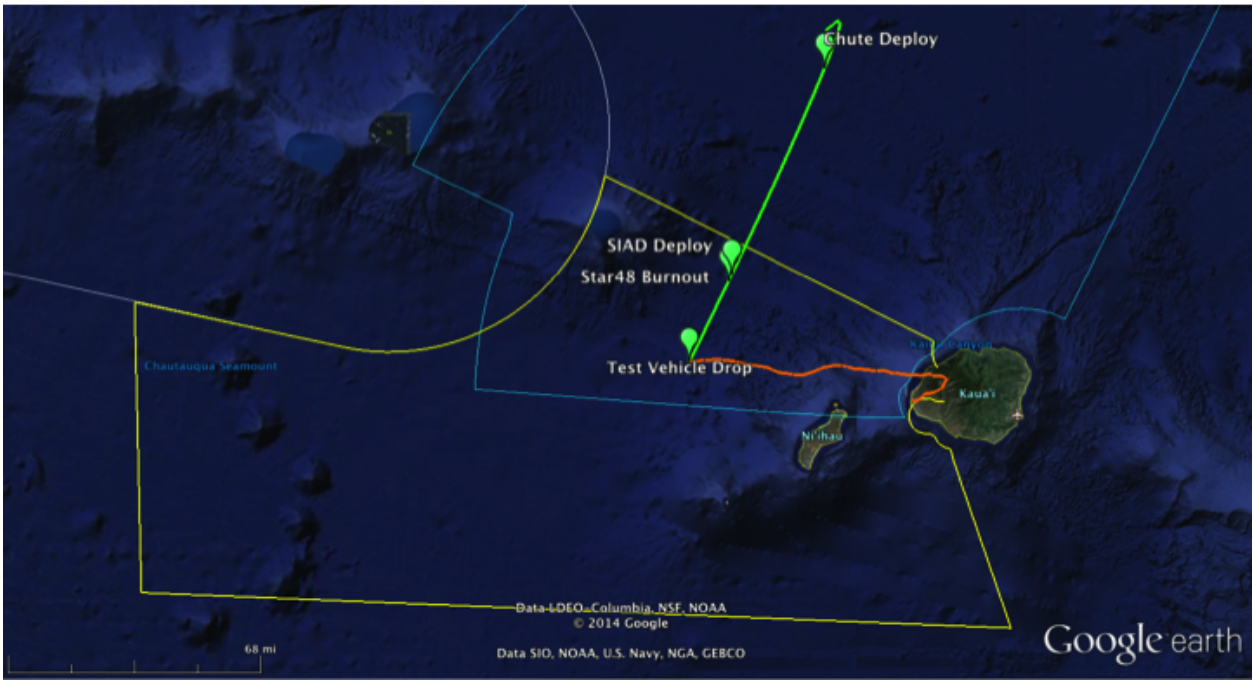

Figure 8. Balloon launch constraints and SFDT1 Ground Track

One day before a potential launch opportunity, a predicted trajectory is generated using the NOAA Global Forecast System model for wind, temperature, and density conditions to feed into a trajectory model. If the predicted trajectory meets the safety and operational constraints, then the launch activities commence that evening for a launch the following morning.

The first launch period for SFDT1 was June 3, 2014 through June 14, 2014. None of those potential launch days were acceptable due to the predicted balloon ascent trajectories violating the safety boundaries over Kauai. The second launch period for which the range was available was June 27, 2014 to July 3, 2014. The first day of the second launch period was used to bring the range and mission systems back to operational status after the two-week hiatus. On that day, a balloon trajectory prediction was made for a launch the following morning, on June 28, 2014, and was found to be acceptable. The launch preparations commenced on the evening of June 27, 2014.

At 11:30 pm HAST the SFDT1 test vehicle was transported from the Missile Assembly Building to the launch site. Once at the launch site shortly after midnight on June 28th, the test vehicle was mated to the balloon gondola hardware on the launch tower. Operations of the mission were controlled by interconnected teams on the range that were at the launch site for balloon activities up to and including launch (Red Label

Area), in the Range Operations Control Center (ROCC) for range systems, recovery, and overall mission direction, the Balloon Operations Center (BOC) for balloon control during ascent, and the Test-Vehicle Operations Center (TOC) for test vehicle commanding and telemetry assessment throughout the mission from pre-launch to splashdown. Figure 9 shows the locations of the facilities on the range. The range telemetry systems are on Makaha ridge.

Figure 9. PMRF Facilities

A series of checkout activities were conducted first with the test vehicle on its ground cart, and later with the vehicle lifted to the launch position. The test vehicle and gondola can be seen in the launch position in Figure 10, with the bottom of the balloon train draped behind the tower. The checkouts verified the operation of the test vehicle and gondola electrical systems, and exercised the radio frequency interfaces with the range. The checkouts were completed at 4:05 am HAST on launch day.

At launch minus 90 minutes, the balloon inflation began, and was completed at launch minus 45 minutes. At launch minus 41 minutes, 8 am HAST, the test vehicle systems were powered up for launch. The umbilicals to the test vehicle were pulled at 8:36 am, and the balloon launched at 8:41 am HAST.

B. Ascent and Drop

The balloon ground track can be seen in red in the Figure 8, which very closely followed the predicted trajectory. The balloon crossed over the coast of Kauai about one hour after launch, at which time it was at an altitude of 18 km. A series of ballast drops were conducted shortly before and after crossing the coast, in order to assure a positive ascent rate through the tropopause. During ascent the predicted time at float altitude was updated in order to prepare for drop shortly after reaching float, and to select a time for drop and a pointing azimuth for the powered-flight trajectory. The drop time selected was 11:05 am HAST. During ascent, the gondola and test vehicle were commanded through UHF receivers on the gondola. The procedure to power up and arm the test vehicle systems for drop began at 40 minutes before drop, with all systems operating as expected.

The balloon reached its final float altitude of 36.55 km at 2 hours and 22 minutes after launch, at 11:03 am. Also at this time the test vehicle GLN-MAC attitude was initialized as the final preparation before

Figure 10. SFDT1 Test Vehicle and Balloon Gondola on Launch Tower

drop. At 11:05 am, as planned, the test vehicle was dropped from the gondola in a fully armed state using a UHF tone broadcast from the range to the Drop Receiver on the test vehicle. After the drop, the balloon was terminated and fell with the gondola to the ocean.

C. Flight

The armed drop initiated a series of autonomous events on the test vehicle, all of which executed as planned. After drop there is no commanding of the vehicle. The test vehicle was tracked by the range using a C-band transponder on board. That location of the vehicle was used to point the range antennas in order to collect real-time telemetry and situational awareness video on S-band through out the flight. The ground track of the flight trajectory is the green line in Figure 8.

The spin-up motors fired at 0.4 and 1.7 seconds after drop to stabilize the vehicle, and main motor ignition occurred at 2.2 seconds after drop. The main motor burned out at 71 seconds after drop, followed by the spin-down motor firings at 72 seconds after drop. At this time the vehicle was traveling at Mach 4.3 at an altitude of 54.6 km. The SIAD-R was deployed 83 seconds after drop at Mach 4.08 at an altitude of 58.2 km. The SSDS was deployed 169 seconds after launch at Mach 2.54 at an altitude of 47.1 km. All of the instrumentation on the vehicle operated as planned and collected and returned the desired data.

In addition, MET rockets were launched from the range from one half-hour before drop to two hours after drop to construct a representative atmosphere model for the time and altitudes of the test. Out of four MET rockets launched, one was successful and one other partially successful, which was sufficient to collect the desired data.

The test vehicle descended to the ocean where it splashed down at 11:35 am HAST, 30 minutes after drop. Telemetry from the vehicle, which included GPS data, was used to predict the splashdown time and location. An altitude switch on the test vehicle autonomously shut down all systems at 15,000 ft above the ocean, in order to safe the vehicle for recovery.

D. Recovery

Recovery vessels were sent out the evening before launch in order to pre-position for recovery of the balloon envelope and the test vehicle. Spotter aircraft were used to assist in locating the balloon envelope and test vehicle in the water. The balloon descent was observed by the spotter aircraft and tracked down to the water. The ballon recovery vessel, the Honua, successfully retrieved the entire balloon envelope and gondola from the ocean from 1:45 pm to 3:30 pm HAST on June 28, 2014, and returned them to port at 7 am the next day for disposal.

The test vehicle and the separable flight image recorder on the test vehicle both have Iridium transmitters that periodically broadcast their GPS locations. That was the primary means of location determination used by the vessels and aircraft. These systems worked as expected, and the test vehicle was quickly located after splashdown. The flight image recorder had the highest priority for recovery, since that data was not telemetered. A fast vessel, the Manao II, arrived at the test vehicle first at 1:45 pm HAST and disconnected and retrieved the recorder in case the test vehicle might sink before it was recovered. On the way to the test vehicle, the Manao II crew spotted the ballute in the ocean, and radioed its location to the test vehicle recovery vessel, the Kahana.

In an unplanned operation, the Kahana recovered the ballute from the ocean at 1:14 pm and then proceeded to the test vehicle, arriving at 2:15 pm. The test vehicle was recovered and on the Kahana at 2:30 pm. The flight image recorder was transferred from the Manao II to the Kahana at that time. The Kahana delivered the recovered test vehicle and flight image recorder to Port Allen on Kauai at 7 am the following day, June 29, 2014. Figure 11 shows the test vehicle recovery.

Figure 11. SFDT1 Test Vehicle Recovery on to the Kahana

V. Test Article Performance

A. Atmosphere & Test Conditions

Knowledge of the atmosphere at the altitudes of interest was achieved via a combination of weather balloons carrying Radiosonde instrumentation and Super Loki meteorological sounding rockets (MetRockets) with PWN-12a ROBINspheres. The former ascended to altitudes between 30 and 35 km while carrying an instrument for measuring pressure, temperature, humidity, and GPS position. The MetRockets deployed an inflatable Mylar sphere that was tracked via radar to back out winds and density, which was subsequently used to derive pressure and temperature. Although four MetRockets were launched, only one ROBINsphere yielded good density and wind data and another was able to provide only wind data.

Reconstructed values of density, temperature, speed of sound, and wind are provided in the figures below.

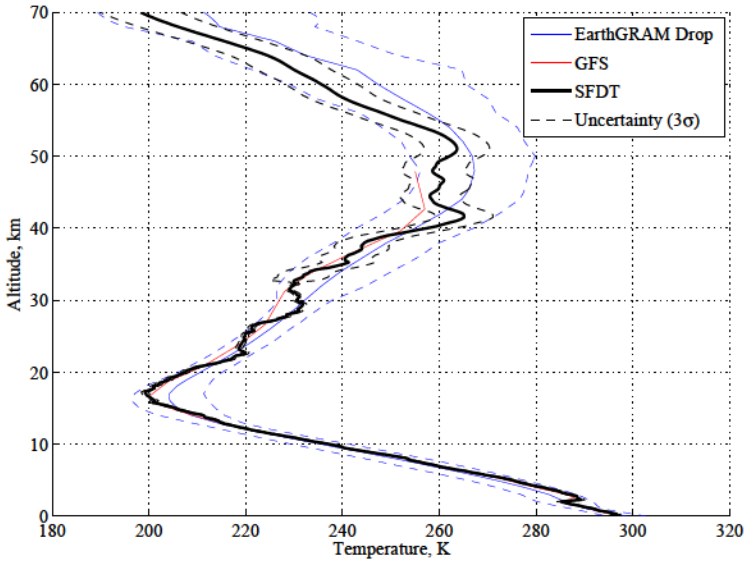

Figure 12. Reconstructed temperature profile with comparison to both EarthGRAM and Global Forecasting System models.

The relevant test conditions are known from post-processing vehicle-sensed and ground-sensed instruments. The data post-processing for SFDT-1 included an Extended Kalman Filter (EKF) that combined the meteorological, IMU, GPS, and radar data. Trajectory conditions at key events were calculated from the reconstructed atmosphere and vehicle trajectory and are summarized in Table 4.

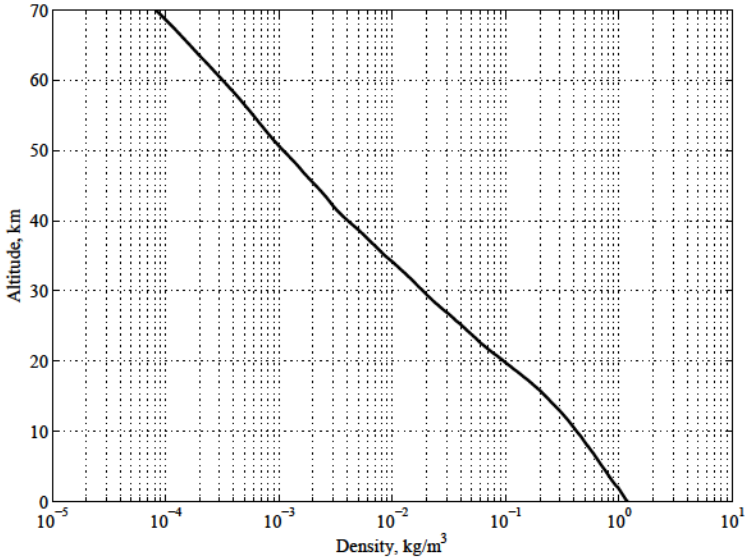

Figure 13. Reconstructed density profile.

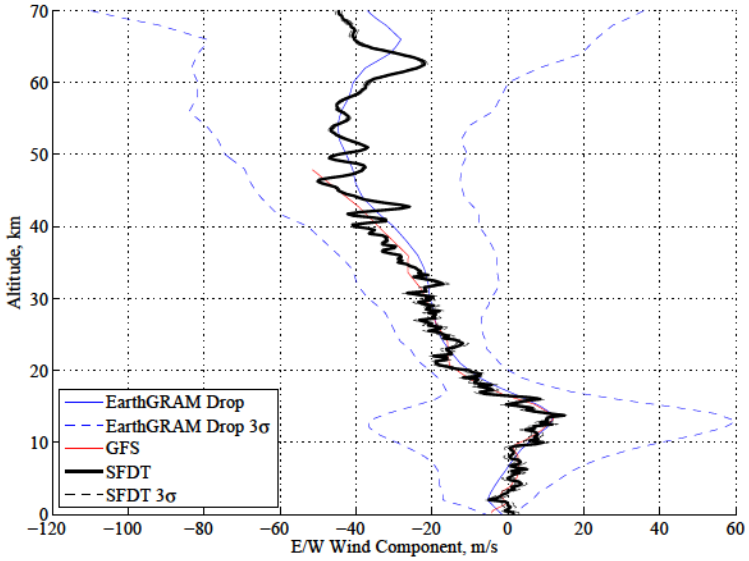

Figure 14. Reconstructed wind component in the east direction.

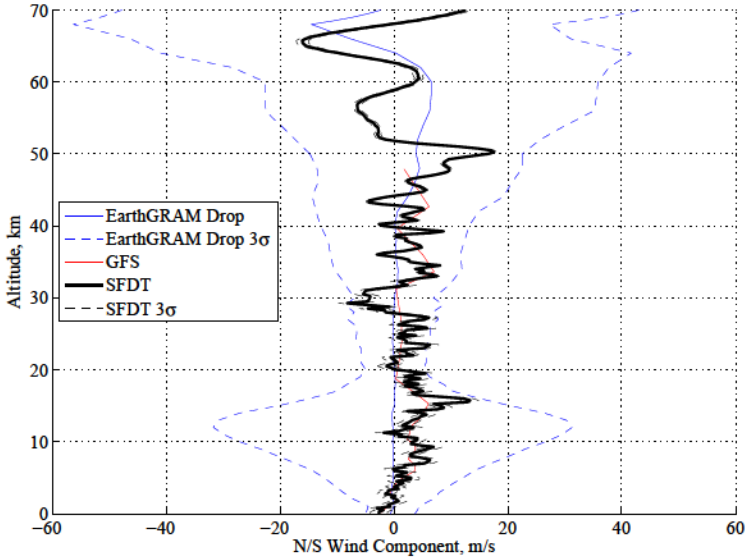

Figure 15. Reconstructed wind component in the north direction.

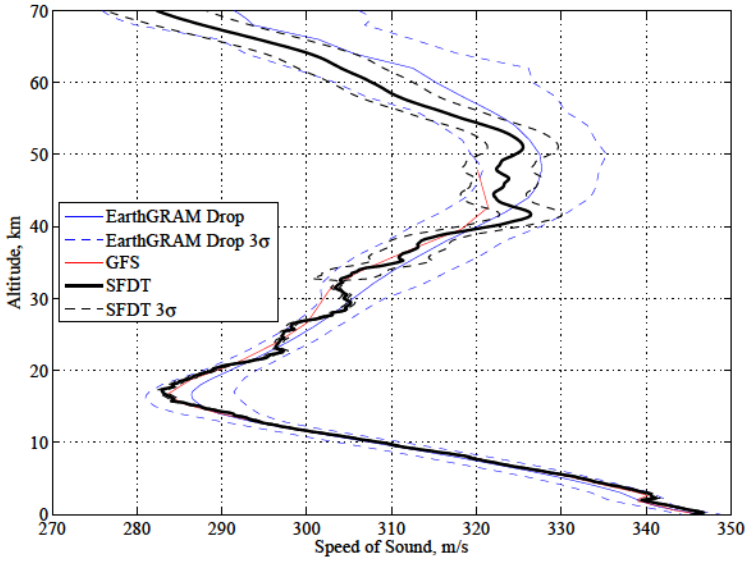

Figure 16. Reconstructed speed of sound profile.

Event *N/A*	**Time from Drop** *sec*	**Mach**	**Dynamic Pressure** *Pa*	**Wind-Relative Velocity** *m/s*	**Geodetic Altitude** *km*	**Mars Eq. Altitude** *km MOLA*	**Flight Path Angle** *deg*
Drop	0.00	0.01	0.02	2.52	36.35	2.06	2.47
Spin up 1	0.37	0.01	0.03	3.08	36.35	2.06	−4.16
Spin up 2	1.67	0.04	0.69	13.91	36.34	2.03	−24.75
Ignite	2.17	0.06	1.12	17.75	36.33	2.01	−30.98
Mach 1	26.26	1.00	240.79	316.38	38.95	4.39	50.55
Mach 2	43.27	2.00	508.40	644.77	43.88	10.35	31.56
Mach 3	57.04	3.00	604.65	968.68	48.79	15.69	23.06
Mach 4	67.77	4.00	632.18	1294.98	52.93	19.89	18.15
Burnout	71.03	4.32	623.00	1385.63	54.23	21.09	16.92
Spin Down 1	72.09	4.30	583.69	1373.28	54.64	21.49	16.53
Spin Down 2	72.60	4.30	567.79	1369.63	54.84	21.72	16.34
VT1 Detection	80.33	4.14	370.91	1291.91	57.43	24.98	13.32
SIAD Deploy	83.00	4.08	324.33	1265.70	58.17	25.92	12.22
VT2 Detection	161.41	2.73	426.05	886.89	50.05	15.17	−27.24
PDD Mortar	161.58	2.73	429.90	886.69	49.98	15.06	−27.33
Bridle Cut	166.57	2.60	507.52	837.62	47.92	11.84	−30.06
SSDS Line Stretch	168.65	2.54	545.14	822.92	47.05	9.58	−31.30
Parachute Inflation	169.30	2.46	525.92	794.94	46.77	10.08	−31.78
Mach 1.4	183.05	1.40	320.11	456.92	41.94	2.88	−43.11
Mach 1.0	194.81	1.00	250.48	315.33	38.66	N/A	−55.34
Mach 0.5	241.47	0.50	234.92	152.60	29.43	N/A	−82.72

Table 4. Trajectory conditions at key test events. VT1 and VT2 correspond to the conditions at the preprogrammed Velocity Trigger points.

B. SIAD-R

1. *Deployment and Inflation*

Deployment of the SIAD was initiated with the firing of pyrotechnic devices that were used to secure a restraint and release system that held the SIAD packed on the periphery of the vehicle. Shortly thereafter a set of nine cold-gas (compressed gas) gas generators (gg's) were fired to provide the initial pressurization of the SIAD. The SIAD subsequently began emerging from its packed configuration out in to a supersonic freestream. The cold gas gg's only provided a fraction of the pressure necessary to achieve a rigid geometry with the SIAD. However, prior ground based testing on 1/9th SIAD models had shown that attempting to provide too large of an initial pressure pulse could lead to emergence velocities and snatch conditions capable of damaging the SIAD. Thus, a two stage inflation process was employed, the initial cold gas gg's sized to provide some initial emergence and loose shape of the SIAD prior to a series of nine hot gas gg's providing the full pressurization. This approach was successfully employed on SFDT-1 with a 0.3 second delay between the two sets of gg's.

Initial emergence of the SIAD was observed to be relatively uniform with no significant asymmetries in geometry observed. Although some flagging of the SIAD is visible from the onboard cameras, it was not easily distinguishable from general inflation and it persisted only until the hot gas gg's were fired, at which point the SIAD appeared effectively rigid. Vehicle motions during deployment were also seen to be negligible, and post-SIAD inflation vehicle dynamics indicated that the SIAD had provided an overall reduction in vehicle oscillations. The progression of the SIAD from a stowed configuration to fully deployed is shown in Figure 17.

A trio of internal pressure transducers recorded the initial rise in pressure associated with the cold gas gg's to a value of approximately 1 psia and later rise from the hot gas gg's to a peak value of about 4.5 psia. Pressure traces from each are shown in Figure 18. After peaking, the inflation gas began cooling and subsequently the pressure decreased to a rough steady state value of around 3 psia. Pressure decay from that point was relatively minor with the SIAD losing less then 0.5 psia over the next three minutes.

2. *Aeroelastic Distortion*

For SFDT-1, a camera internal to the SIAD was present that was used to track the position of three LEDs installed on the wall of the SIAD. This was subsequently used to track the aeroelastic distortion of the SIAD by measuring the displacement of the LEDs in the plane of the image. During the deployment of the SIAD, the LEDs did not emerge in the field of view of the internal camera until the firing of the hot gas gg's. However, within 0.25 seconds of the hot gas gg's being activated the LEDs were indicating a value of defection of only two mm. A general trend was observed in aeroelastic deflection that showed a nearly linear relationship with the freestream dynamic pressure at supersonic conditions. That is, for the flown SFDT-1 trajectory, SIAD deployment occurred with a positive flight path angle and subsequently waning dynamic pressure. After vehicle apogee, the dynamic pressure began building back up and observed aeroelastic deflection began increasing up to the point of parachute deployment. Peak defections of approximately 12 mm were seen to coincide with PDD mortar fire and peak parachute loading and were likely due to the shock loads induced by both events.

A summary of the defections measured during SIAD flight is shown in Figure 19 along with a linear correlation with dynamic pressure. The linear correlation holds very well up until transonic and subsonic conditions, after which the deflection is nearly constant. This result is likely associated with a change in aftbody pressure on the SIAD that occurs as the vehicle goes subsonic and thus a differing aerodynamic torque on the SIAD.

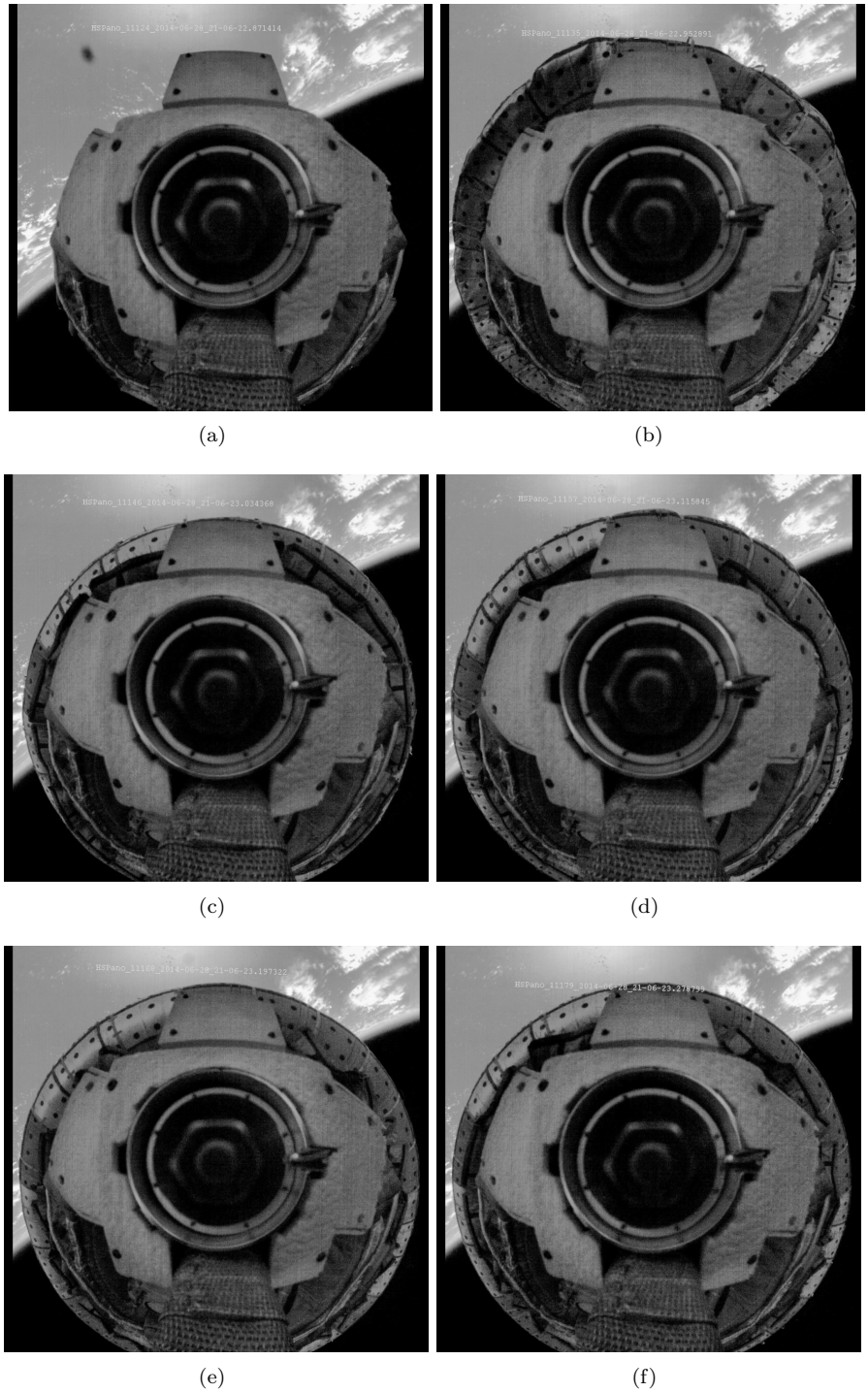

Figure 17. Progression of SIAD inflation from a complete stowed state (a) to a visibly rigid shape (f), progressing in 81.48 ms increments.

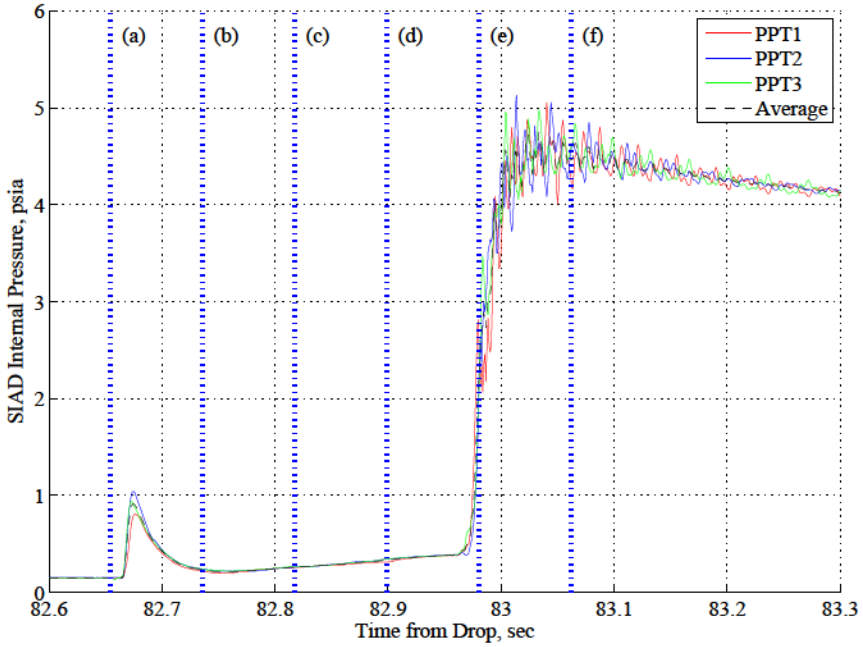

Figure 18. SIAD internal pressure history during initial moments of inflation. Vertical blue lines and associated letters correspond to subimages shown in Figure 17.

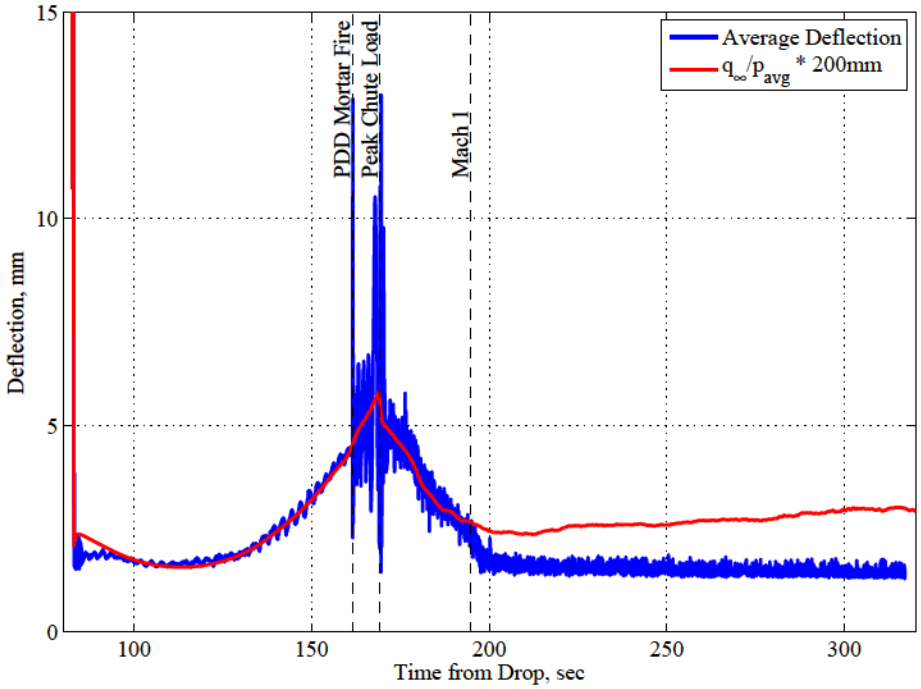

Figure 19. Average deflections of the three LEDs compared to a scaled ratio of freestream dynamic pressure and average internal pressure.

3. *Aerodynamics and Aerothermodynamics*

With regards to the aero- and aerothermodynamic performance, SIAD-R met or exceeded expectations. The reconstructed static force and moment aerodynamic coefficients are shown in Figures 20 and 21 along with the preflight aerodatabase values associated with the vehicle state at each moment. Axial force coefficient for the test vehicle prior to SIAD deployment was approximately 1.55 and approximately 1.35 immediately after SIAD deployment. Though the axial force coefficient decreased, a net increase in drag area ($C_D A$) of approximately 42% was achieved.

Overall agreement with axial force coefficient predictions is excellent and generally within a few percent. The largest deviations occur as the vehicle is reaching apogee and may be due to the aerodatabase generally being constructed from CFD analyses conducted for lower altitude conditions. The reconstructed side force coefficients also shows excellent agreement, however, the signal to noise ratio in vehicle accelerations in those axes is significantly lower than for axial forces and the uncertainties associated with the reconstructed values are relatively large. A similar situation is evident in the moment coefficients, where there is excellent agreement between nominals, though the reconstructed uncertainties are large percentages of the nominal value.

Due to the lack of any significant disagreement with the preflight aerodatabase, and predictions of stability by the aerodatabase, it is concluded that the deployed SIAD-R configuration was statically stable. Time histories of the wind relative angles are also indicative of a vehicle that is either dynamically stable or possesses only a slight instability above Mach 3.0.

The SIAD was instrumented with a number of externally and internally mounted thermocouples to track inflation gas temperatures and assess the aerothermal environment encountered. Internal gas temperature measurements were used to understand gas generator exhaust temperatures and if any appreciable surface heating affected the internal gas temperature. A peak internal temperature of around 60 °C was recorded at a time coincident with the hot-gas gg firing. Preflight estimates of hot-GG exhaust temperatures were approximately 375 °C, significantly higher than the observed peak. However, the response rate of the TC's is such that they were not capable of measuring a very transient peak in temperature. No appreciable rise in internal gas temperature was observed for the remainder of the test period.

Overall, SIAD surface temperatures were seen to be relatively benign and lower than pre-flight estimates, with peak recorded temperatures of less than 120 °C. The low temperatures likely resulted from two primary contributors, the lofted trajectory and lower than expected thermal response from the SIAD. In the case of the former, although the Mach number at deployment was above 4, the altitudes and densities were lower than nominal predictions, reducing the aerothermal heating environment. With regards to the thermal response of the SIAD, this is likely a combination of heat rates lower than predicted, even at the higher altitudes, and challenges in the modeling of the thermal response of the SIAD.

The highest measured temperatures for all thermocouples occurred at roughly the same time, around Mach 2.0. An assessment of the as-flown trajectory using preflight aeroheating indicators was performed and indicated that the highest heat rates likely occurred just prior to parachute deployment and line stretch. The difference in time between estimated peak heating and peak measured temperatures thus points to a fair amount of lag in the thermal response of the SIAD material. Given the use of high-denier Kevlar and silicone coating, along with increased thermal mass associated with TC installation, this is not unexpected. Highest temperatures were consistently recorded at a location on the windward side of the SIAD burble, in a region predicted to experience some of the highest heat rates.

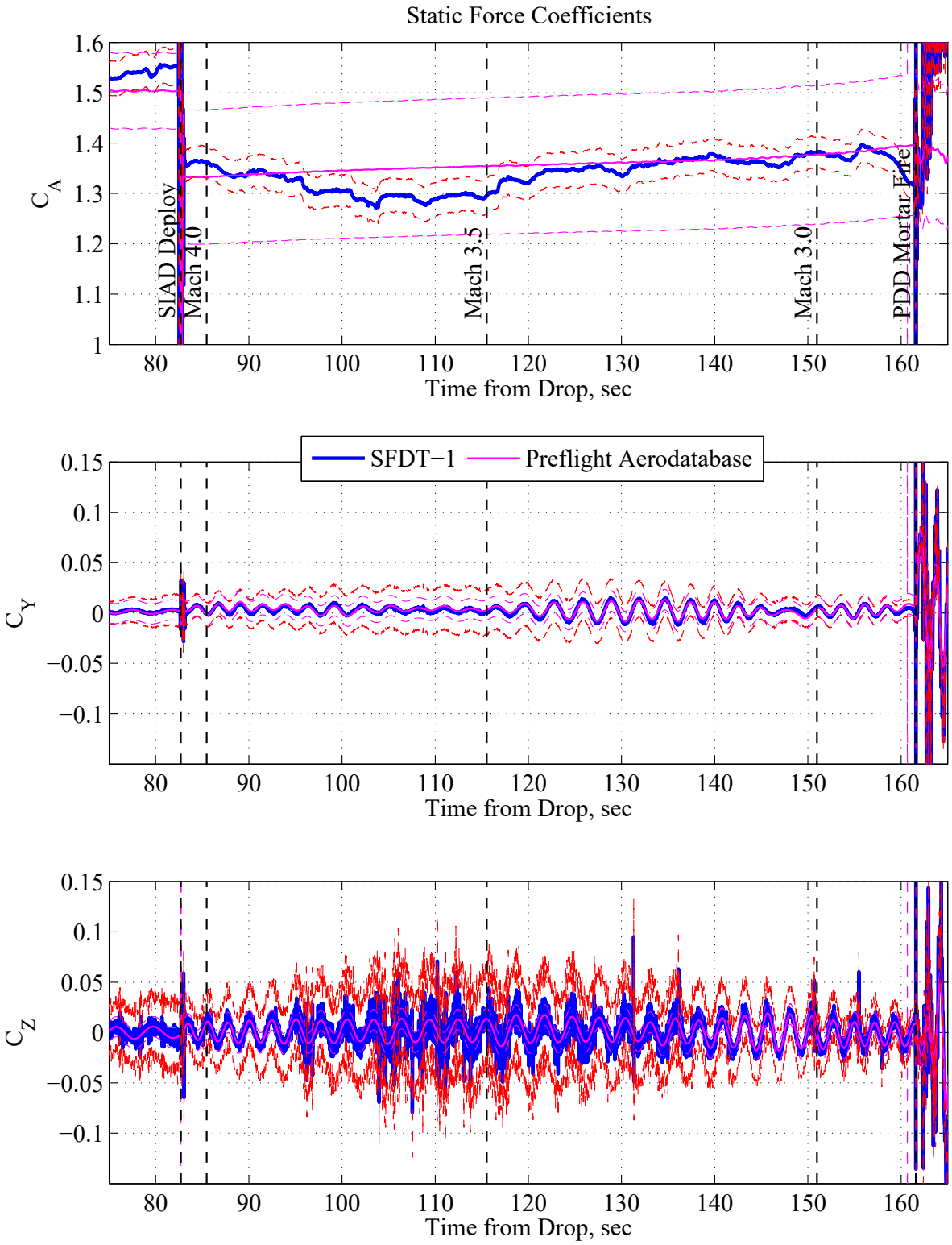

Figure 20. Reconstructed and preflight aerodatabase static force coefficients during SIAD flight. Dashed red lines correspond to the 3σ uncertainty values from reconstruction.

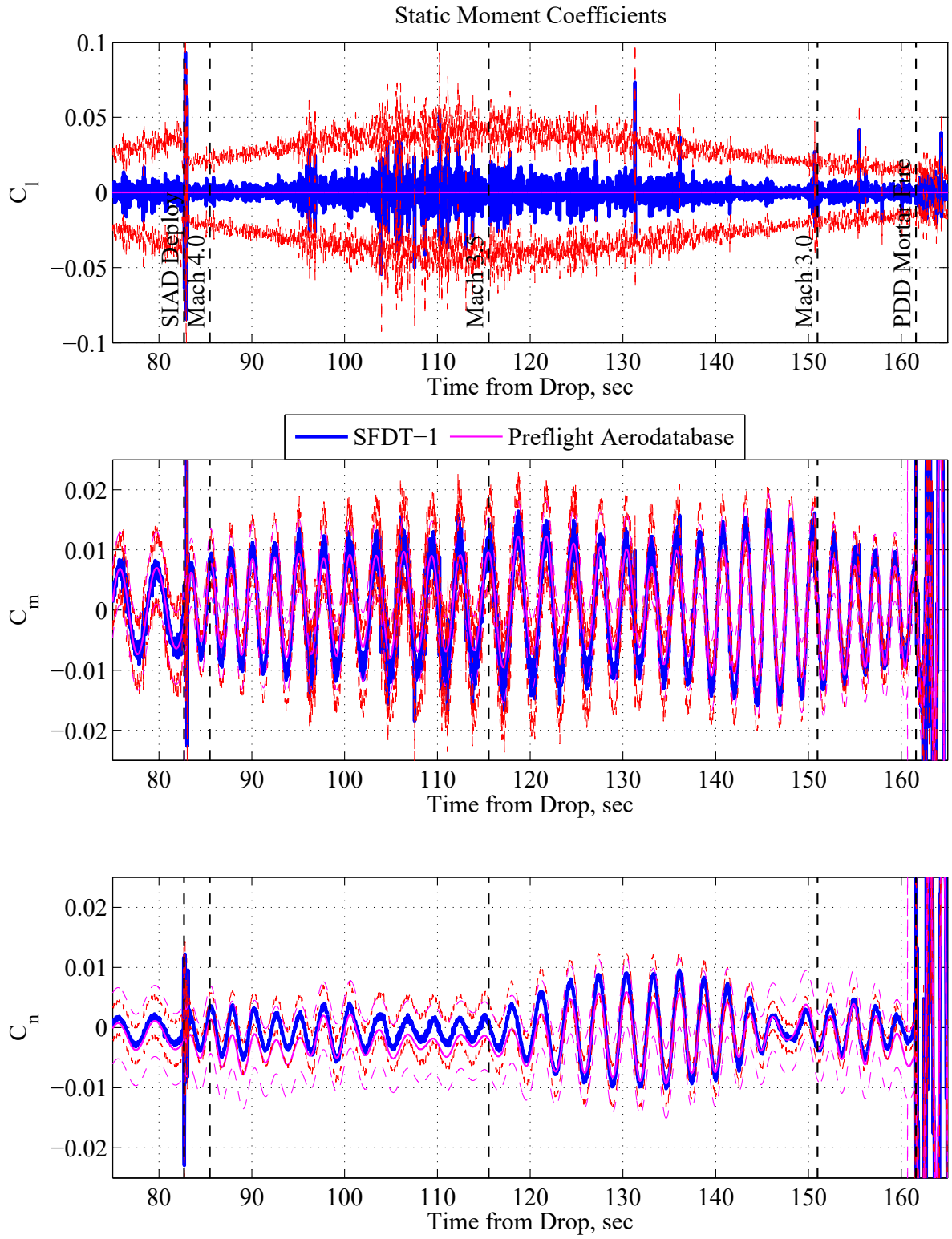

Figure 21. Reconstructed and preflight aerodatabase static moment coefficients during SIAD flight. Dashed red lines correspond to the 3σ uncertainty values from reconstruction.

C. Parachute Deployment Device

Prior to SFDT-1, the PDD was considered one of the riskiest items of the entire test. Schedule and resource limitations had restricted ballute development to rely heavily on computational tools to estimate aerodynamics, aerothermodynamic environments, and local stresses. No aerodynamic wind tunnel tests were conducted and no overall structural testing was performed on a full scale ballute. Ground testing was largely limited to inflation aid development tests, mortar testing, coupon testing, and a few truck-tow tests. However, during SFDT-1, the LDSD ballute performed above expectations in both its measured drag and observed stability.

As mentioned previously, ballute inflation was initiated at line stretch by the use of an inflation aid containing an aqueous water/alcohol mixture. After initial inflation, ram-air inlets are exposed to the oncoming flow to provide the remaining pressurization and to help maintain pressurization as dynamic pressure changes. The ballute inflation process is shown in Figure 22 from just prior to line stretch to full inflation. Post-test estimates of the inflation aid performance using known flight conditions calculated that the inflation aid provided nearly all of the initial pressure necessary to inflate the ballute. However, because the ballute stayed fully inflated during flight and was recovered inflated from the ocean, it is believed that the ram-air inlets were effective. Furthermore, imagery shows the eight raised inlets to be fully deployed and pressurized during ballute operation.

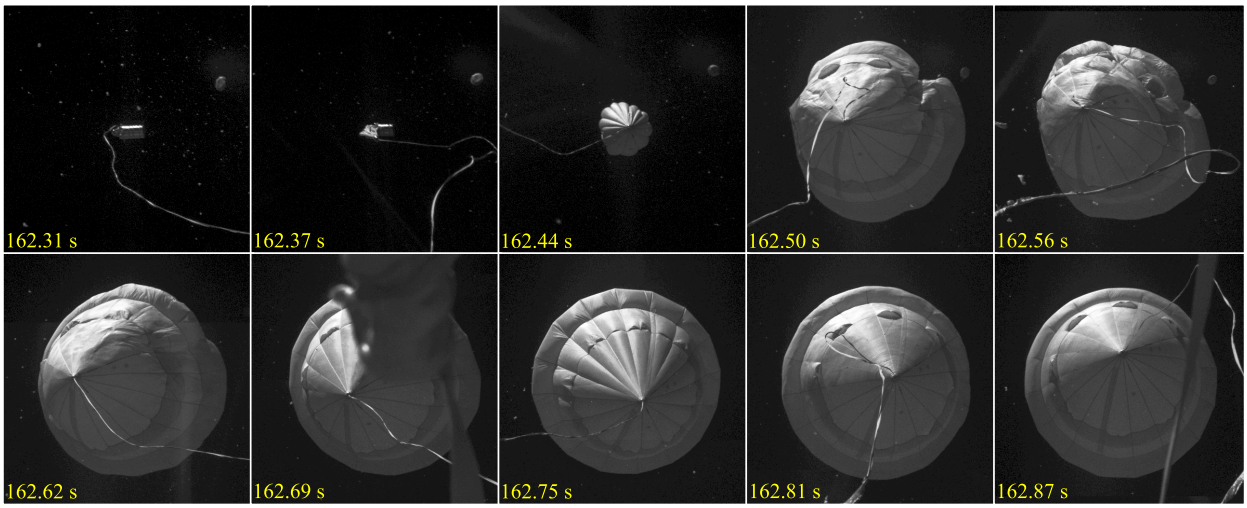

Figure 22. Ballute inflation sequence as shown from just prior to line stretch to full inflation. The reconstructed seconds from drop is indicated in each image.

The dynamics of the ballute after inflation were characterized by initially large pitch and yaw rotations of the ballute and oscillatory loads that damped out over a few seconds. The ballute trails the maximum diameter of the inflated SIAD by 42 m, or 7 forebody diameters, and the ballute resides in a highly turbulent, blunt body supersonic wake environment. Thus, some dynamic motion was expected from the ballute. Load cell data from the ballute, shown in Figure 23, shows several large initial peaks associated with high snatch forces as the ballute initially inflated and subsequently rebounded. These damped out and eventually an average ballute force of approximately 1000 lbf was measured.

The load pin data was used to calculate a ballute total force coefficient and drag coefficient, where the former is the force acting along the pull direction of the ballute and the latter is the force in the wind relative direction. This data, as a function of Mach number, is shown in Figure 24. The calculated drag coefficient was generally higher than pre-flight CFD estimates. Early analysis of the data indicates that this is likely due to the stability of the ballute and its position in the wake of the test vehicle. Specifically, the pre-flight drag estimates were based on CFD of the ballute in the wake centerline, where the dynamic pressure deficit is largest. Analyses of the ballute at small angles of attack had been run and shown that the ballute would have a large restoring force to push it back to the centerline. During the flight the ballute did not fly precisely on the centerline and pull angles of between 5 and 10 degrees were measured. At those angles, the ballute would have seen a higher local dynamic pressure environment and thus provided more drag.

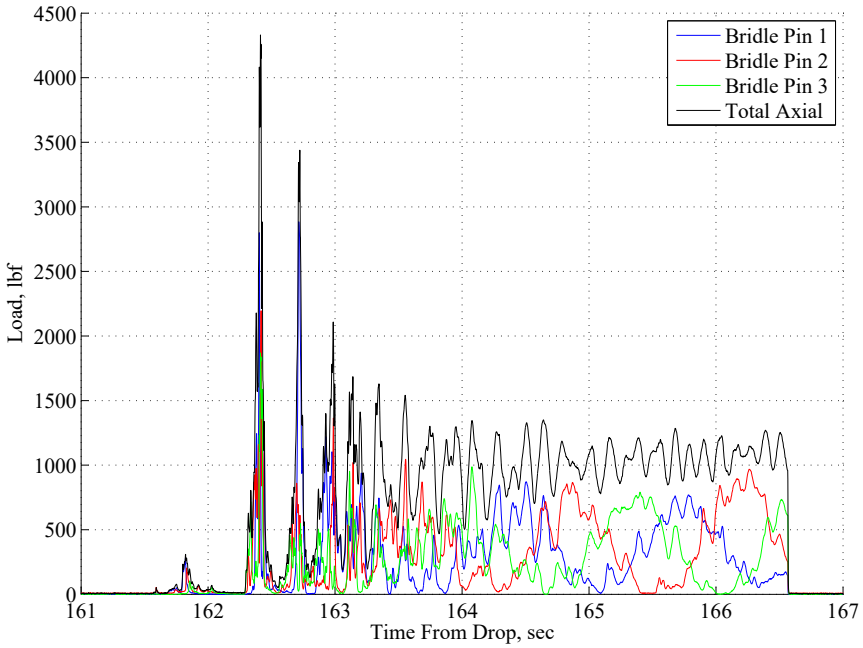

Figure 23. Ballute load history. The first force peak near 161.8 seconds is the triple bridle standup snatch.

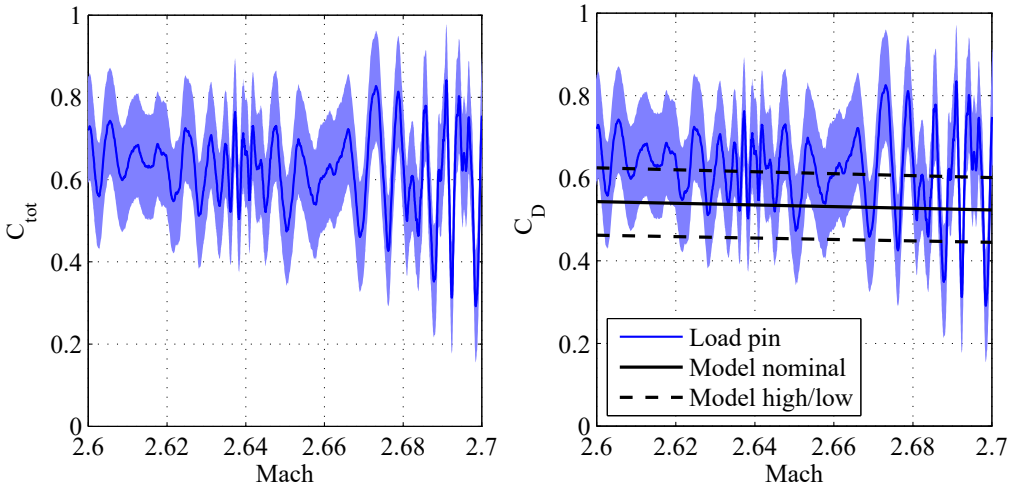

(a) (b)

Figure 24. Ballute total force coefficient (C_{tot}) reconstructed from load pin measurements, and pre-flight predicted ballute drag coefficient (C_D) as a function of wind-relative Mach number for the last 3 seconds of ballute flight. The shaded regions indicate the 3σ confidence interval on C_{tot}, and the dashed lines indicate the high and low bounds in the preflight C_D prediction.

D. Supersonic Disksail Parachute

Deployment of the parachute began when the ballute triple bridle was cut and the ballute began pulling the parachute pack off of the back of the test vehicle. Extraction of the parachute from triple bridle cut to parachute line stretch occurred over 2.08 seconds. During this time the parachute bridles were deployed and the suspension lines emerged from the parachute pack. Prior to line stretch the suspension lines appeared orderly though the snatch force at line stretch induced a transverse wave that subsequently induced more disorganization. Initial emergence of the canopy from the parachute pack also appeared orderly.

Initial inflation of the parachute, shown in Figure 25 appeared to proceed in a manner typical of low-density supersonic inflation with very fast initial motions, significant line dynamics, and elements of asymmetrical inflation visible. However, very early on in the inflation process canopy damage is visible and the tears propagate further until at peak inflation the canopy has significant damage throughout. The canopy continued to destroy itself over the next second.

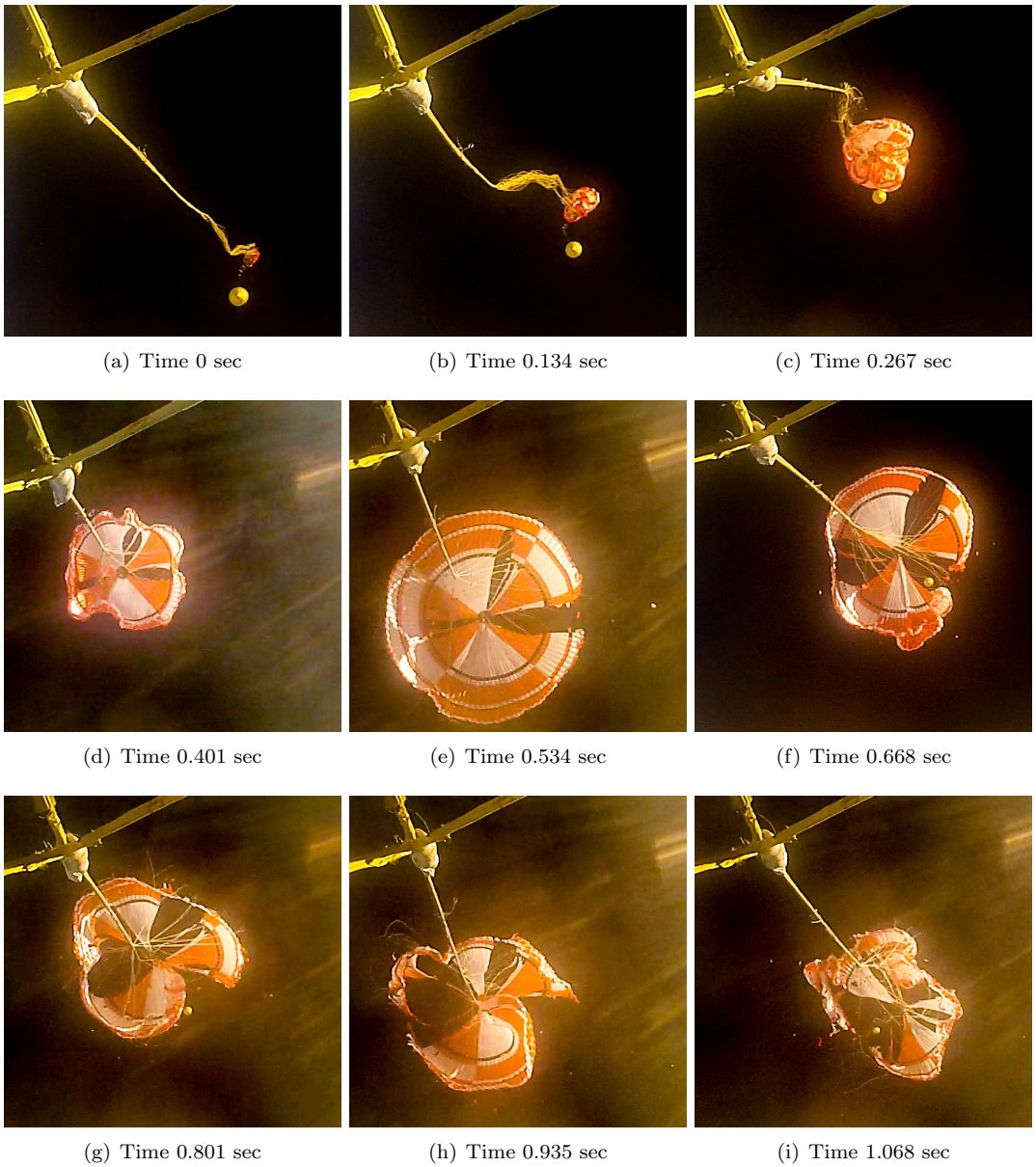

(a) Time 0 sec (b) Time 0.134 sec (c) Time 0.267 sec

(d) Time 0.401 sec (e) Time 0.534 sec (f) Time 0.668 sec

(g) Time 0.801 sec (h) Time 0.935 sec (i) Time 1.068 sec

Figure 25. Image sequence during canopy inflation. Note that the time reference is arbitrary.

Closer inspection of the high speed imagery captured during flight indicated that the initial location of damage appeared in the disk region of the parachute (see Figure 26) and quickly propagated radially towards the vent and to the edge of disk. At the time of initial damage visibility, windowing in the disk fabric can also be identified and later frames showed the windowing transitioning to more significant radial tears. By [illegible]nt, with

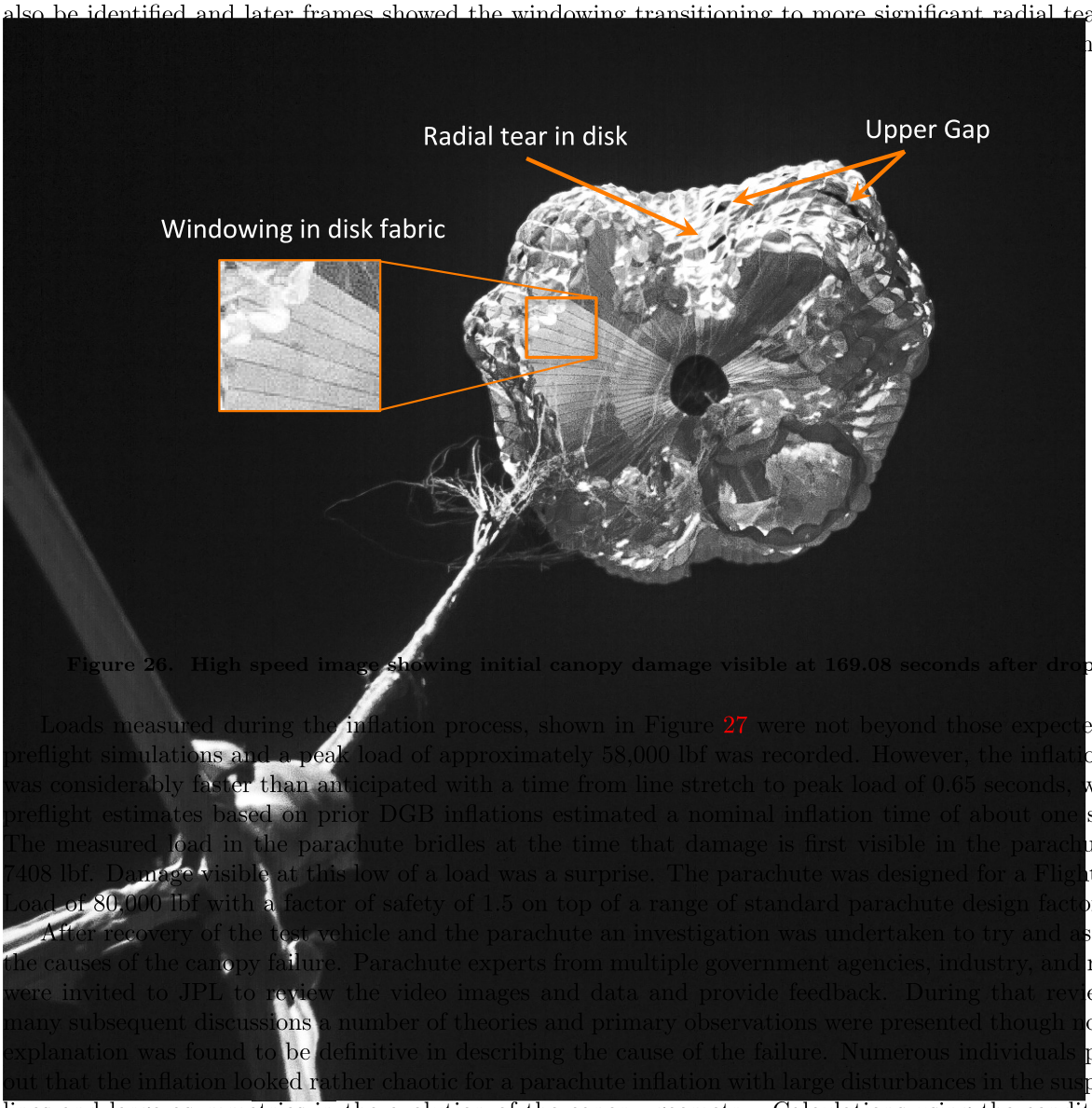

Figure 26. High speed image showing initial canopy damage visible at 169.08 seconds after drop.

Loads measured during the inflation process, shown in Figure 27 were not beyond those expected from preflight simulations and a peak load of approximately 58,000 lbf was recorded. However, the inflation time was considerably faster than anticipated with a time from line stretch to peak load of 0.65 seconds, whereas preflight estimates based on prior DGB inflations estimated a nominal inflation time of about one second. The measured load in the parachute bridles at the time that damage is first visible in the parachute was 7408 lbf. Damage visible at this low of a load was a surprise. The parachute was designed for a Flight Limit Load of 80,000 lbf with a factor of safety of 1.5 on top of a range of standard parachute design factors.

After recovery of the test vehicle and the parachute an investigation was undertaken to try and ascertain the causes of the canopy failure. Parachute experts from multiple government agencies, industry, and retirees were invited to JPL to review the video images and data and provide feedback. During that review and many subsequent discussions a number of theories and primary observations were presented though no single explanation was found to be definitive in describing the cause of the failure. Numerous individuals pointed out that the inflation looked rather chaotic for a parachute inflation with large disturbances in the suspension lines and large asymmetries in the evolution of the canopy geometry. Calculations using the conditions at line stretch also indicated that there was likely some rebound of the canopy at line stretch, with an estimate of just less than 2 m. In response to the feedback of a chaotic inflation event, JPL reviewed, with the collected experts, most of the existing video on low-density supersonic parachute inflations, video collected during the PEPP, SPED, and SHAPE test programs. As those videos were rewatched it became clear that many of the behaviors seen in SFDT-1 were typical of a supersonic parachute inflation, including the line dynamics, canopy rebound, and asymmetric inflation. Furthermore, additional behaviors were gleaned from the 1960's footage that previously were not observed due largely to the quality of the video. Having the significantly higher resolution SFDT-1 footage allowed for even greater insights into those prior tests.

Although many suggestions and factors were presented during the discussions, most of them could either be discounted or eliminated as being sole reasons for the parachute failure. Some of these are itemized below with additional hypotheses as to why they are either relevant or not.

- **Test Conditions:** None of the trajectory related test conditions, e.g. Mach number, dynamic pressure, flight path angle, etc., were outside of the range of expectations for the test. Additionally, the peak load measured was well within the expected loads for these conditions.

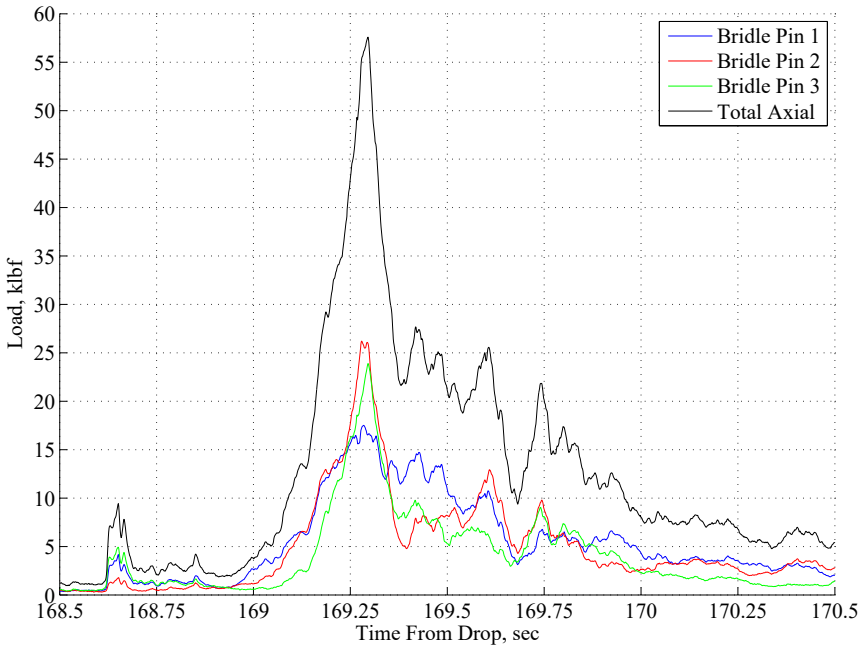

Figure 27. Measured parachute bridle loads during inflation.

- **Aerothermal Heating:** It is well known that lightweight parachute broadcloth is susceptible to heating at supersonic Mach numbers and recent experience with supersonic parachutes fabricated from Nylon and Kevlar, namely the Mars missions of the past two decades, has generally not exceed a Mach number of 2. Using the Mach and atmosphere conditions at line stretch, the freestream stagnation temperature would have been 595 K while the minimum melting temperature of Nylon yarn is only 517 K. Though this could be a concern, parachute test programs of the 1960's successfully deployed parachutes at Mach numbers well above that of SFDT-1 using broadcloth material similar to Nylon. For example, Reference 10 and Reference 11 both provide examples of parachutes fabricated almost entirely of Dacron Polyester successfully being flown at Mach numbers of 2.72 and 2.95 respectively. Although the Dacron used was slightly heavier than the Nylon used in the SFDT-1 Disksail, 2.0 oz/yd^2 versus 1.2 oz/yd^2, Dacron has a melting temperature very similar to that of Nylon. In at least one example where aerothermodynamic heating was identified as a primary contributor to canopy damage, Reference 12, that damage occurred after deployment at Mach 3.31 and not until a full second after the initial opening of the parachute. The lessons learned from historical parachute testing seem to indicate that it is unlikely that the parachute broadcloth acheives stagnation temperatures and that even lightweight cloth still takes some period of time to achieve temperatures where damage would occur. Lastly, upon inspection of the recovered parachute, no obvious signs of aerothermal damage were found. Some signs of heating damage to the canopy could be found, but they appeared of a nature more likely associated with friction burns from the cloth whipping itself after the initial failure of the disk.

- **Asymmetric Inflation:** Ideally, parachutes inflate in a symmetric and orderly manner without false apexes large regions of asymmetry. Large asymmetries during inflation can induce significantly larger local stresses in regions of the parachute that are not designed to handle them. Even quasi-symmetric inflations can lead to significant stress augmentations. In a post-test study of the Disksail canopy using FEA, it was noted that even a symmetric but tri-lobed inflation geometry could produce stresses significantly higher than under a nominal fully inflated geometry. However, videos from the PEPP, SPED, and SHAPE test campaigns show that rapid, asymmetric inflation is common for low-density supersonic parachutes and in that regard the SFDT-1 inflation was no different. Thus, it is difficult to

assign asymmetric inflation as a sole or primary contributor to the observed failure.

- **Line Entanglement:** During the inflation of the parachute some hesitation in the skirt of the canopy was observed and is visible in the lower right of Figure 26. From the video, it appeared that there have been a momentary snag in either the leading edge of the skirt or in the suspension lines in that region. The canopy would eventually recover and inflate fully in that region, but the possibility remains that the snag helped contribute to asymmetry and augmentation of stresses within the canopy.

- **Canopy Rebound:** As was noted previously, estimates based on the conditions at lines stretch are that the canopy would have rebounded approximately two meters after line stretch and during the very earliest part of inflation. This would introduce a period of time where the canopy was inflating without significant radial tension in the system, something which could help explain the low measured loads in the bridle legs at the moment of first visible damage. Though not something that would directly cause a canopy failure, the lack of tension in the system during inflation is generally not desirable as it also may allow for greater asymmetry and localized stresses.

- **Snatch Forces Within the Canopy:** The inflation of the SFDT-1 Disksail canopy occurred in less than 0.7 seconds. The rapid inflation could have led to large snatch forces being generated within the canopy as portions inflated and took shape. Given the location of initial damage, how early it occurred, and that the damage initially occurred in a moderately elastic Nylon broadcloth, this explanation also seems lacking for a primary cause of damage. This kind of damage would seem to be more likely to occur closer to full inflation where more of the canopy has had time to accelerate to higher velocities and more of the snatch forces would be carried by low-elasticity structural Kevlar members.

- **Bag Strip Damage:** One of the more prominent failures of a supersonic parachute occurred during the Viking Balloon Launched Decelerator Test (BLDT) campaign. During the first supersonic inflation, significant canopy damage was observed that was ultimately determined to most likely have occurred during inflation of the parachute.[13] Specifically, an over test in dynamic pressure condition led to a situation where the parachute began inflating prior to bag strip having been completed. The additional frictional forces along with the constrained geometry during inflation damaged the broad cloth significantly. However, the SFDT-1 line stretch velocity was very similar to line velocities achieved during earlier LDSD ground based extraction testing for which no canopy damage was observed. Furthermore, additional care was taken to line the SFDT-1 parachute bag with less abrasive Spectra material to prevent frictional damage.

- **Manufacturing:** Though it is difficult to eliminate manufacturing or workmanship entirely, there is also little evidence to support this as being a primary contributor. No significant deviations in the standard manufacturing and inspection processes were taken during the building of the SFDT-1 canopy.

- **Configuration:** Ultimately the primary hypothesis on the SFDT-1 parachute failure was based on the specific parachute configuration flow, namely a Disksail. A key feature of the Disksail is that an otherwise traditional quarter-spherical Ringsail parachute has the upper portion replaced with a flat disk. Noting that a parachute is functionally a pressure vessel, the primary means of developing large stresses are having a large pressure differential across the membrane, having a large local radius of curvature, or inducing large snatch forces in the canopy. During the inflation of the SFDT-1 Disksail, the disk region is pressurized very quickly but the shoulders of the parachute are also pressurized quickly and move radially outward until being arrested by the constructed geometry. In this situation it is possible that the shoulders of the canopy can pull the disk flat, thus generating a significantly larger radius of curvature than what would be seen when the canopy was already fully inflated. Though no side view of the parachute is available, no significant lobing of the disk is visible in Figure 26 and it appears likely that the disk was relatively flat at the moment of initial damage. It is worth noting that a flat disk is also a feature of the DGB canopy and no DGB failures have been diagnosed in a similar manner. The hypothesis for this is as follows. Although a DGB parachute also incorporates a flat disk, the primary difference with the Disksail is the proportion of flat disk to the rest of the canopy (smaller than for a DGB) and a shoulder region of the parachute capable of generating enough force to flatten the disk during inflation. By the time the band region of a DGB begins being pressurized,

the disk has already begun taking full shape and considerable radial forces are present to prevent the disk from taking too flat a geometry.

The complications associated with supersonic parachute inflation make it difficult to ascertain definitively the cause of the SFDT-1 parachute failure. However, as of this writing the leading hypothesis is a parachute configuration that was fundamentally not suited for the rapid inflation characteristics of a low-density, supersonic inflation. Other hypotheses remain and though they seem less likely, they may still have been contributors.

VI. Summary

On the morning of June 28th, 2014, a supersonic flight test vehicle was launched via balloon from the Navy's Pacific Missile Range Facility on the west In a little over two hours, the balloon reached float altitude over the Pacific Ocean. Two minutes later, the test vehicle was dropped from the balloon at an altitude of 36.4 km. The test vehicle then carried out a series of autonomous activities that began with the firing of small rockets to spin up the vehicle and then a large rocket to accelerate the vehicle to Mach 4.3 at an altitude of 54.2 km. The vehicle was spun down with another set of small rockets. Then two supersonic decelerator technology experiments were conducted.

At Mach 4.08, at an altitude of 58.2 km and a dynamic pressure of 324 Pa, an attached 6-meter SIAD was deployed around the 4.7-meter diameter test. The SIAD performed as expected with a rapid deployment, maintaining a rigid shape with less than 5 mm deflection from the dynamic pressure. The drag area of the vehicle was increased by 42% upon SIAD deployment, in good agreement with the pre-flight predictions. The stability of the test vehicle was improved with the deployment of the SIAD, with the magnitude of oscillations reduced from 3° to less than 2°. Post-flight inspections revealed that no thermal damage to the SIAD was incurred as a result of its operation.

At Mach 2.73, at an altitude of 50.0 km and a dynamic pressure of 430 Pa, a trailing 4.4-meter ballute was deployed. The ballute performed very well, at the high end of its predicted drag. The ballute then pulled out and deployed a 30.5-meter nominal diameter supersonic Disksail parachute. The parachute reached line stretch at Mach 2.54, at an altitude of 47.1 km and a dynamic pressure of 545 Pa. The parachute inflated rapidly in the supersonic flow but showed signs of significant damage to the parachute very early in the inflation process. The damage propagated quickly, culminating in the skirt band breaking within 0.6 seconds after line stretch. The parachute reached a state of full inflation 0.67 seconds after line stretch, with a well-defined shape despite the broken skirt band, but then proceeded to immediately lose shape and rapidly disintegrate in the supersonic flow. The leading hypothesis of the failure of the parachute is related to the Disksail configuration being fundamentally unsuited for supersonic inflation.

The remains of the parachute provided enough drag to keep the vehicle upright on its descent into the ocean and to allow the vehicle to survive the impact with the water largely intact. Two ships conducted a recovery operation with the participation of Navy Explosive Ordnance Divers that successfully retrieved the test vehicle, the parachute, and the ballute, and returned them for inspection. A third ship recovered the deflated balloon envelope that was floating in another part of the ocean, for disposal.

The primary purpose of the flight test was to demonstrate the supersonic test architecture and to provide data and lessons learned to improve future flights. The objectives were to launch the system and reach float altitude, drop the test vehicle and conduct the powered flight, return telemetry from the test vehicle in flight, and recover the balloon envelope for disposal. All of those objectives were met, with all of the expected telemetry collected.

The test vehicle architecture performed as expected in all areas, except that the test vehicle lofted to the very high end of the pre-flight statistical distribution of altitude, resulting in a higher Mach and lower density deployment of the SIAD than targeted. All SIAD objectives were achieved nevertheless, and the reconstructed test vehicle trajectory provided information on the thrust profile of the main rocket motor and the aerodynamic coefficients of the test vehicle that will be used to improve the targeting on later flights. The lofting did not impact the targeted initial test conditions for the supersonic parachute.

The two technology experiments were not objectives of this first flight, but the opportunity was taken advantage of to get early data on the performance of the decelerators. The recovery of the test vehicle and test articles was also not an objective for this first flight, but the successful recovery of particularly the flight image recorder on the test vehicle, the SIAD, and the parachute enabled a thorough investigation of the results of the technology experiments. That investigation has resulted in an early completion of the SIAD-R

technology development, and exposed new phenomenon in the deployment of supersonic parachutes. The knowledge gained will be used to improve the parachute technology for subsequent flights, and will reduce the time it will take to complete that development through its later supersonic flight demonstrations.

Acknowledgments

The Low Density Supersonic Decelerator technology demonstration mission is sponsored by the National Aeronautics and Space Administration's Space Technology Mission Directorate. The authors thank the LDSD team across the participating government facilities and industrial contractors for helping to advance these technologies for the next generation of Mars landers.

A portion of the research described in this paper was carried out at the Jet Propulsion Laboratory, California Institute of Technology, under a contract with the National Aeronautics and Space Administration.

References

[1]Moog, R. D. and Michel, F. C., "Balloon Launched Viking Decelerator Test Program Summary Report," NASA Contractor Report CR-112288, March 1973, pp. 1–82.

[2]Cook, B. T. and et al, "High Altitude Supersonic Decelerator Test Vehicle," AIAA Paper 2013-1353, 2013.

[3]Giersch, L., Rivellini, T., Clark, I., Shook, L., Ware, J., and Welch, J., "SIAD-R: A Supersonic Inflatable Aerodynamic Decelerator for Robotic missions to Mars," AIAA Paper 2013-1327, 2013.

[4]Coatta, D., Jurewicz, D., Tutt, B., Rivellini, T., and Clark, I., "Development and Testing of an 8 Meter Isotensoid Supersonic Inflatable Aerodynamic Decelerator," AIAA Paper 2013-1328, 2013.

[5]Gallon, J. C., Clark, I. G., Rivellini, T., Adams, D., and Witkowski, A., "Low Density Supersonic Decelerator Parachute Decelerator System," AIAA Paper 2013-1329, 2013.

[6]Mitcheltree, R. A., Bruno, R., Slimko, E., Baffes, C., Konefat, E., and Witkowski, A., "High Altitude Test Program for a Mars Subsonic Parachute," AIAA Paper 2005-1659, 2005.

[7]Witkowski, A., Kandis, M., Bruno, R., and Cruz, J. R., "Mars Exploration Rover Parachute System Performance," AIAA Paper 2005-1605, July 2005, pp. 1–8.

[8]Mayhue, R. J. and Eckstrom, C. V., "Flight-Test Results From Supersonic Deployment of an 18-Foot-Diameter (5.49-Meter) Towed Ballute Decelerator," NASA Technical Memorandum TM X-1773, May 1969.

[9]Usry, J., "Performance of a Towed 48-Inch-Diameter (121.92-cm) Ballute Decelerator Tested in Free Flight at Mach Numbers From 4.2 to 0.4," NASA Technical Note TN D-4943, Feb. 1969.

[10]Eckstrom, C. V. and Preisser, J. S., "Flight Test of a 40-Foot-Nominal Diameter Disk-Gap-Band Parachute Deployed at a Mach Number of 2.72 and a Dynamic Pressure of 9.7 Pounds Per Square Foot," NASA Technical Memorandum TM X-1623, Aug. 1968, pp. 1–43.

[11]Eckstrom, C. V., "High-Altitude Flight Test of a 40-Foot-Diameter (12.2-Meter) Ringsail Parachute at a Deployment Mach Number of 2.95," NASA Technical Note TN D-5796, June 1970, pp. 1–51.

[12]Eckstrom, C. V., "Flight Test of a 40-Foot-Nominal-Diameter Disk-Gap-Band Parachute Deployed at a Mach Number of 3.31 and a Dynamic Pressure of 10.6 Pounds Per Square Foot," NASA Technical Memorandum TM X-1924, Feb. 1970, pp. 1–49.

[13]Dickinson, D., Hicks, F., Schlemmer, J., Michel, F., and Moog, R. D., "Balloon Launched Decelerator Test Program Post-Flight Test Report: BLDT Vehicle AV-1," NASA Contractor Report CR-112176, Sept. 1972, pp. 1–199.